ACS Editors' Choice

Terms of Use

ARTICLE

Fabrication of Corona-Free Nanoparticles with Tunable Hydrophobicity

Daniel F. Moyano,[†] Krishnendu Saha,[†] Gyan Prakash, Bo Yan, Hao Kong, Mahdieh Yazdani, and Vincent M. Rotello*

Department of Chemistry, University of Massachusetts Amherst, 710 North Pleasant Street, Amherst, Massachusetts 01003, United States. [†]D.F.M. and K.S. contributed equally to this work.

ABSTRACT A protein corona is formed at the surface of nanoparticles in the presence of biological fluids, masking the surface properties of the particle and complicating the relationship between chemical functionality and biological effects. We present here a series of zwitterionic NPs of variable hydrophobicity that do not adsorb proteins at moderate levels of serum protein and do not form hard coronas at physiological serum concentrations. These particles provide platforms to evaluate nanobiological behavior such as cell uptake and hemolysis dictated directly by chemical motifs at the nanoparticle surface.

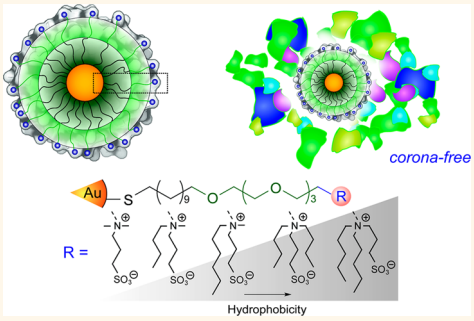

KEYWORDS: corona-free NPs · hydrophobicity · cellular uptake · hemolysis · interfacial tension · sedimentation · dynamic light scattering

Surface functionalization of nanoparticles (NPs) is an essential tool to modulate the behavior of these materials both *in vitro* and *in vivo*.[1,2] The biodistribution,[3] toxicity,[4] and clearance[5,6] of nanomaterials can be regulated through controlled chemical modifications. However, when NPs are exposed to biofluids, such as plasma or serum, proteins and other biomolecules adsorb on the surface of these materials (Figure 1a).[7−9] This *in situ* formation of a "protein corona"[10,11] masks the engineered functionalities on the nanoparticle surfaces, dramatically changing the nature of their interaction with biosystems.[12−14] For example, the targeting efficacy of antibody-functionalized NPs are compromised due to the high levels of opsonization.[15,16] Likewise, the study of correlations between surface functionality and biological activity is challenging, as the results are subject to the interplay between the chemical moieties and the corona, rather than depending on the functionalities themselves.[17,18]

Many approaches have been investigated to prevent the formation of the protein corona to provide NPs with nonfouling properties. One classical approach is the use of a noncharged poly(ethylene glycol) (PEG) polymer that prevents the NP from adsorbing proteins.[19,20] However, it has been observed that PEG-functionalized NPs do indeed interact with certain plasma proteins, inducing the activation of different immune responses.[21] Moreover, systematic changes in the surface properties of PEG-functionalized NPs are difficult to achieve as the absence of charge allows the internalization of pendant hydrophobic functionalities, reducing exposure.[22] An alternative to the use of PEG is the incorporation of zwitterion functionalities onto the NP surface, including amino acids[23] and polybetaines.[24] The strong electrostatic binding of water with zwitterions (as opposed to water hydrogen bonding with PEG) has been postulated as the rationale behind the high degree of stability and nonfouling properties observed with zwitterionic systems.[25] However, pH dependence of carboxy-based systems[26] and the difficulty of systematic functionalization[27,28] limit the ability to control surface properties while maintaining biocompatibility and corona-free character.

Herein, we report the synthesis and use of a new family of NP surface coverages that exhibit tunable hydrophobicity while

* Address correspondence to rotello@chem.umass.edu.

Received for review February 1, 2014 and accepted June 27, 2014.

Published online June 27, 2014
10.1021/nn5006478

© 2014 American Chemical Society

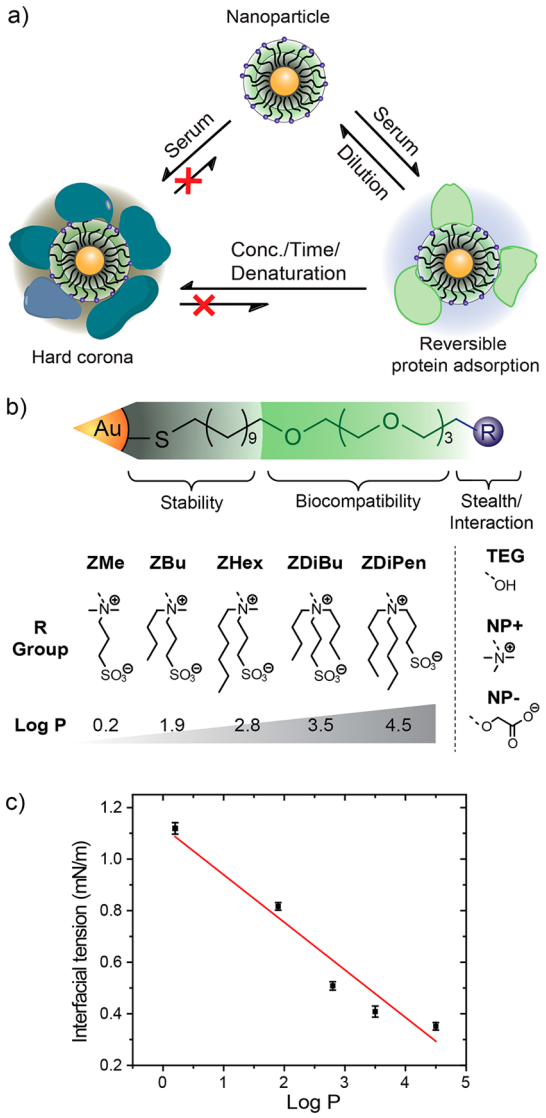

Figure 1. (a) Reversible adsorption of proteins and formation of irreversible hard corona over the NP surface. (b) Structures of the nonfouling NPs, along with TEG, NP+, and NP− controls. The ligand structure consists of a hydrophobic interior that confers stability to the NP core, an oligo(ethylene glycol) chain used as a first layer for biocompatibility, and the zwitterionic headgroups to confer ultrafouling properties. The zwitterionic headgroups (the NP surface) differ only in their hydrophobicity, whose relative values can be estimated by the calculated log *P* of the terminal functionality. (c) Correlation of the calculated log *P* with toluene/water interfacial tension.

preventing the formation of a protein corona. This nanoparticle ligand design maintains corona-free behavior at moderate protein levels and prevents the irreversible formation of "hard" corona at physiological serum concentrations, while allowing properties such as hydrophobicity to be varied. These "naked" particles allow a systematic molecular structure-based assessment of the effects caused directly by the NP surface, including cellular uptake and hemolytic activity.

RESULTS AND DISCUSSION

The chemical design of the NP ligand is based on a combination of a short oligo(ethylene glycol) spacer with sulfobetaine termini (Figure 1b). This combination has been shown to provide better stealth properties to NPs compared to the ethylene glycol chains alone.[29] Hydrophobicity was chosen as the chemical variable due to the significant role played by this parameter at the nano−bio interface, including protein−NP interaction,[30,31] cellular uptake,[18] toxicity,[32,33] and immune system recognition.[34,35] The degree of surface hydrophobicity was controlled with these ligands by systematically engineering the quaternary ammonium nitrogen (Figure 1b, synthesis and characterization described in the Supporting Information, Figures S1−S11). All particles were fabricated from a 2 nm gold core, a factor that contributes to the observed corona-free character, given the reduced protein adsorption[7] and the increased plasma stability of small nanoparticles.[36] In addition, these NPs offered us a suitable system for structure−activity relationship (SAR) studies, as the physicochemical parameters of the NPs, such as the hydrodynamic radii and zeta-potential, remained constant (Table 1).

A numerical descriptor is commonly employed in SAR studies to represent the property that is being tested. Computational calculation of the *n*-octanol/water partition coefficient of the NP headgroups (log *P* of R groups, Figure 1b) provides a readily accessible means to describe the relative hydrophobicity of NPs.[37] These calculated values were correlated with water/toluene interfacial tension (IFT) measurements, a technique that has been used to describe the effective surface hydrophobicity of NPs independent of the material of origin.[38] As can be observed in Figure 1c, the calculated log *P* values and the experimental IFT results are essentially linearly correlated, indicating that the hydrophobicity of the NPs is predicted by the log *P* descriptor. The very low threshold of values of the IFT of these NPs evidenced their high degree of amphiphilicity, a characteristic that is on favor of their colloidal stability despite the overall neutral zeta-potential. ZDiPen represents the limit in terms of hydrophobicity: if the log *P* of the headgroup is above 4.5 (IFT < 0), or if the length of the straight-chain substituents is larger than six carbons, the NPs were insoluble in water.

To determine the preliminary interactions of the synthesized NPs with proteins,[26,39] dynamic light scattering (DLS) measurements were recorded in the presence of 1% serum, the highest concentration that did not overwhelm the NP signal (Figure S13; experiment also performed in 1% plasma, Figure S15). The principal change in the DLS profile of serum after the addition of NP+ (cationic), NP− (anionic), and TEG (neutral oligo(ethylene glycol)-capped particles) was the shift of the ∼9 nm hydrodynamic diameter (d_h) peak to ∼20 nm, evidencing the formation of discrete protein−NP complexes, namely, the protein corona (Figure 2a,b). For NP+, the formation of a peak above 1000 nm was also

TABLE 1. Nanoparticle Physicochemical Properties

nanoparticle	hydrodynamic size (nm) in water	hydrodynamic size (nm) in PBS	hydrodynamic size (nm) in cell culture media	zeta-potential (mV) in 5 mM PB pH 7.4	zeta-potential (mV) in water	calculated log *P* of the ligand headgroup
ZMe	6.7 ± 1.1	7.9 ± 2.0	8.4 ± 1.5	−6.8 ± 5.5	−17.9 ± 5.0	0.2
ZBu	8.1 ± 1.6	7.8 ± 1.5	7.2 ± 1.9	−7.7 ± 5.9	−15.6 ± 3.4	1.9
ZHex	8.4 ± 2.1	7.9 ± 1.6	8.7 ± 2.3	−2.9 ± 8.9	−19.8 ± 3.5	2.8
ZDiBu	7.2 ± 1.9	8.3 ± 1.9	7.3 ± 1.9	−5.6 ± 9.3	−14.8 ± 7.2	3.5
ZDiPen	7.2 ± 1.8	7.6 ± 1.9	6.9 ± 1.9	−5.4 ± 9.1	−17.8 ± 3.7	4.5
NP+	9.7 ± 2.8	9.0 ± 2.6	9.6 ± 2.7	16.9 ± 13.6	45.1 ± 10.0	
NP−	6.9 ± 2.1	7.6 ± 1.8	7.0 ± 1.9	−28.2 ± 4.9	−54.7 ± 13.6	
TEG	7.0 ± 1.8	8.6 ± 2.9	6.7 ± 1.7	−0.9 ± 7.6	8.4 ± 5.9	

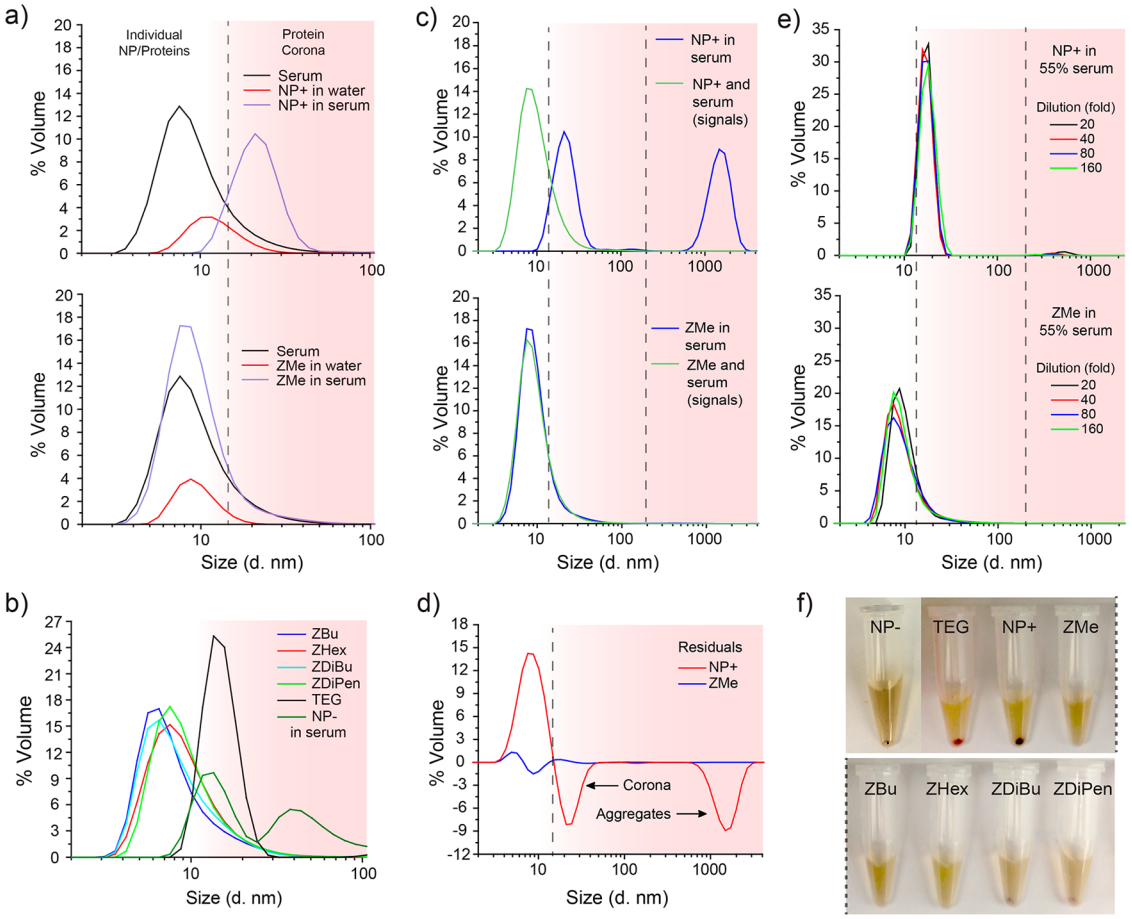

Figure 2. (a) Particle size distribution for cationic NP+ and zwitterionic particle ZMe in the presence and absence of serum proteins (1% serum, background) evidencing the formation of NP/protein complexes (~20 nm) with NP+ but not with ZMe (complete spectra and additional analysis in plasma in Supporting Information). (b) Lack of corona formation for zwitterionic particles in serum and corona formation for TEG (lacking zwitterionic headgroup) and anionic NP−. (c) Comparison between the experimental DLS profiles of each NP in serum with the additive histogram of the combination of the individual serum and NP. (d) Residuals of the spectra in serum after removing the individual NP and serum histograms, evidencing corona and aggregate formation for NP+ with minimal residual observed for ZMe (additional NPs in Figure S14). (e) Dilution studies showing lack of hard corona formation for ZMe after incubation in 55% human serum, with contrasting behavior by the cationic NP+ particle. (f) Sedimentation experiments for the series of NPs in 55% plasma showing that zwitterionic NPs ZMe to ZDiPen did not aggregate, in contrast to NP+, NP−, and TEG that formed pellets.

observed, indicating the presence of extended protein−NP aggregates (Figure S13). In contrast, only the peak at ~9 nm was observed with the zwitterionic NPs ZMe to ZDiPen (Figure 2a,b). These results can easily be contrasted by comparing the predicted histogram in the case where no corona is formed (the addition of the individual serum and NP histograms) with the experimental DLS distribution after mixing the NPs with serum (Figure 2c). As observed in Figure 2d, the subtraction of the experimental histograms from the predicted additive histograms shows that while NP+ presents residuals at the ~20 and ~1000 nm zones

indicative of both aggregation and corona formation, ZMe has minimal residual, indicating the absence of corona at these protein levels (additional NPs in Figures S14 and S16).

Corona formation involves both reversible and irreversible (hard corona) adsorption of proteins on the NP surface (Figure 1a).[40−42] While we were unable to verify the lack of reversible protein adsorption at physiological serum concentrations, we were able to verify the absence of hard corona formation on zwitterionic NPs through incubation and dilution. For this purpose, we incubated the set of NPs with 55% human serum at 37 °C for 30 min, diluted the solutions, and recorded DLS measurements to observe if irreversible protein−NP interactions had occurred for the controls and if crowding effects may alter the absence of corona for the zwitterionic NPs. As observed in Figure 2e, although the peak of the NP−protein conjugates (>1000 nm) for NP+ decreased when the sample was diluted, the peak at ∼20 nm that describes discrete NP−protein complexes remained present after dilution, indicating a strong irreversible protein binding (hard corona). Similar results were obtained for NP− and TEG, suggesting that the larger protein−NP conjugates dissociated and only the discrete ones remained after dilution (Figure S17). In contrast, for NPs ZMe−ZDiPen (Figures 2e and S17), the ∼9 nm peak was the only one observed, indicating the absence of an irreversible protein layer (hard corona).

Further studies using electrophoresis established that zwitterionic particles ZMe−ZDiPen are noninteracting in plasma (55% in PBS, v/v), a more complex matrix. As expected, the mobilities of cationic NP+ and anionic NP− were affected by the presence of proteins due to the corona formation. In contrast, similar mobilities were observed for the zwitterionic NPs in the presence and absence of plasma proteins (Figure S18). Likewise, TEG presented a minimal difference between the two conditions, and the subtle band movement in the presence of protein presumably occurs due to NP aggregation. Despite these results, gel electrophoresis does not provide a definitive result on the absence of corona formation due to the poor mobility of all of the NPs in the agarose matrix. To further corroborate our hypothesis, sedimentation experiments were performed in the presence of 10%, 55%, and undiluted plasma, mimicking *in vitro* and *in vivo* conditions.[42] As expected, while NP+ formed a pellet, NPs ZMe to ZDiPen presented minimal or no aggregates even at physiological plasma levels (Figure 2f and Figure S19a, with no pellets formed even under ultracentrifuge conditions). These qualitative observations were validated by UV measurements of the supernatants before and after the sedimentation process (Figure S19b). NP− presented a pellet of smaller size than NP+, a result that correlates with the observations by DLS and gel electrophoresis. Significantly, TEG NP presented sedimentation similar to the one observed for NP+. This outcome mirrors the results from DLS experiments and is consistent with previous findings that postulate the recognition of PEG functionalities by proteins of the bloodstream.[21]

We wanted to observe if we were able to obtain pellets for the zwitterionic NPs using other variants of the sedimentation experiments and also confirm that the sedimentation of NP+ was due to the formation of corona and no simple NP precipitation. To this end, we repeated the sedimentation experiments using different sucrose gradients, a technique that has been used to separate NP/protein complexes from NPs alone.[14] Under these conditions, we obtained similar results as with the direct sedimentation experiments, with a thick pellet only observed for NP+ (Figure S20a). We further ran a SDS-PAGE gel treating all the samples as if precipitation was observed, and from the results, it can be observed that NP+ did adsorb proteins over the surface while ZMe−ZDiPen behave as the negative control (serum only, no NPs added, Figure S20b). This further confirms the absence of irreversible protein adsorption over the surface of zwitterionic NPs at physiological protein levels. It is important to note that we did observe a very faint precipitation for the more hydrophobic NPs; however, this precipitate was redissolved in the washing steps with PBS (intended to remove loosely bound proteins). This result indicates that even if NP/protein interactions are observed at large values of hydrophobicity, these interactions are reversible and no hard corona is formed.

Once the absence of corona was established, we investigated the effects of NP hydrophobicity on cellular uptake,[43] a phenomenon critically affected by the NP surface and the protein corona.[44−46] For this purpose, uptake studies were performed in serum-containing and serum-free media, conditions that critically affect the trend of uptake of NPs of varying hydrophobicity.[18] As seen in Figure 3a, there was an increase in cellular uptake with increasing surface hydrophobicity for both cases. In previous studies, when NPs were exposed to the cells in serum-free conditions, increasing hydrophobicity increased cell uptake, similar to the results that we obtained.[18] However, when the studies were performed in media with serum, increasing the hydrophobicity of NPs led to greater protein adsorption over the NP surface,[47] which in turn reduced the cellular uptake.[48,49] In contrast to these prior systems, we obtained similar cellular uptake trends for NPs ZMe−ZDiPen both in the presence and in the absence of serum. This result indicates that direct correlations between the NP surface chemistry and biological responses can be assessed with these NPs, providing further proof of the absence of proteins on the NP surfaces and the direct presentation of the chemical motifs to the cellular environment. As expected, overall uptake was low[50] and there was a

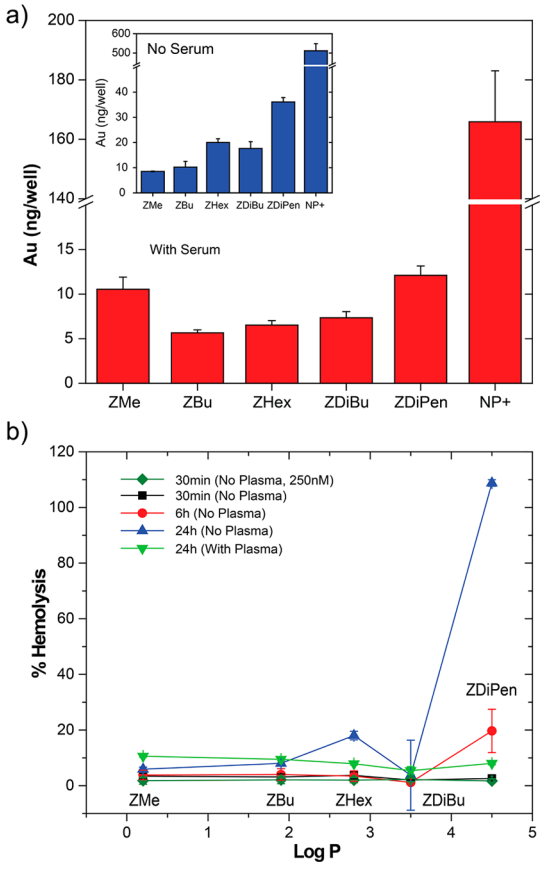

Figure 3. (a) Cellular uptake (MCF7 cells, 3 h) of zwitterionic NPs ZMe to ZDiPen and NP+ in presence and absence (inset) of serum, showing similar uptake trends for both experimental conditions (24 h result in Figure S21). (b) Hemolytic activity of the NPs at different time points and in the presence and absence of plasma (NPs at a concentration of 500 nM unless otherwise stated).

marked difference in the absolute amount of NP uptake in the presence and absence of serum (~2-fold higher uptake without serum). This latter phenomenon has been observed previously for other particles independent of their charge,[51,52] possibly due to nonspecific binding of proteins and NPs to the cell membrane, a competitive process that slows the uptake of NPs when proteins are present.[17,52] This phenomenon may be the rationale behind the fact that the trend of cellular uptake with NP hydrophobicity in serum was more evident at 24 h (Figure S21). Finally, it is important to note that at the conditions of the study the nanoparticles were noncytotoxic (Figure S22).

Due to the corona-free character, these NPs have the potential for long blood circulation times,[53] increasing the possibility of hemolytic activity. As such, hemolytic assays were performed as a means to probe the compatibility of the NPs with red blood cells (RBCs).[54,55] NPs ZMe to ZDiPen were incubated with RBCs isolated from commercially purchased human whole blood. The experiments were performed both in the presence and in the absence of blood plasma.[56] The results (Figure 3b) provide evidence that no significant cell lysis was elicited by the zwitterionic NPs either in the presence or in the absence of plasma. Hemolytic activity was only observed for the more hydrophobic NP (ZDiPen) at 24 h without plasma proteins, consistent with a critical change in the behavior of NPs at extreme values of hydrophobicity. However, it is important to note that during the half-life that is expected for these particles (~6 h),[29] no significant hemolytic response was observed in the presence of plasma proteins for the zwitterionic NPs.

CONCLUSION

In summary, we have demonstrated that sulfobetaine headgroups can be engineered to provide particles with controlled hydrophobicity. These particles do not adsorb proteins at moderate serum protein concentrations nor do they form a hard corona at physiological serum conditions. The ligand design provides the potential to directly control the interaction of the nanomaterials with biosystems without interference from protein binding. As such, these coverages provide promising scaffolds for delivery vehicles and self-therapeutic systems. They also open new avenues for probing the fundamental nature of the nano–bio interface through direct interfacing of synthetic and biological components without intermediary complications arising from the protein corona.

METHODS

Nanoparticle Synthesis and Characterization. Please refer to the Supporting Information for a detailed description of the ligand synthesis, nanoparticle functionalization, and characterization.

Interfacial Tension. The dynamic interfacial tension of the NPs at the toluene–water interface was measured by the pendant drop method using an OCA20 measuring instrument (Dataphysics, Stuttgart). A syringe filled with an aqueous solution of NPs (1 μM) connected to a blunt needle was fixed vertically with the needle immersed in the toluene phase. A small amount of solution was injected from the syringe to form a drop. The variation of drop shape with time until equilibrium (interfacial tension) and drop fall was captured by automated camera. The measurements were performed in triplicate.

Dynamic Light Scattering. DLS profiles were recorded in 1% human serum (~16 μM protein concentration) diluted in phosphate buffered saline (PBS, pH 7.4) at 37 °C with NPs at a concentration of 1 μM using a Malvern Zetasizer Nano ZS. For the dilution profiles, NPs at a concentration of 50 μM were incubated for 30 min at 37 °C in 55% human serum, then diluted accordingly. The subtraction of the individual NP and serum spectra from the "NP in serum" results was done point by point using normalized data to take into account the concentration of each species (spectra of individual NPs and serum reported as normalized). The results are reported as % number when individual NPs are analyzed (characterization) and as % volume for the NP/protein mixtures due to the dependence on the different refractive index of each entity.

Sedimentation. To a solution of 10 and 55% plasma (in PBS) and undiluted plasma, NPs were added to achieve a final concentration of 500 nM (500 μL total volume). The solutions were incubated for 5 min, and the tubes were subjected to centrifugation for 30 min at 14 000 rpm. After centrifugation, 200 μL of the supernatant was transferred to a 96-well plate alongside 200 μL of the same mixture before the centrifugation. The absorbance values were measured at 506 nm, which is the wavelength at which NP concentration is determined. The absorbance generated by the proteins was subtracted using a blank protein sample with no particles. UV differences were significant only at 10% plasma, as the proteins have much more interference at 55% plasma. All NPs and blank samples were prepared in triplicate. For the sucrose gradients, NP samples in undiluted serum/plasma were centrifuged at 14 000 rpm for 30 min using a sequential gradient of 24, 12, and 6% sucrose and a sharp gradient of 24% for the gel. Ultracentrifugation experiments were run at 60 000 rpm for 1 h.

Agarose Gel Electrophoresis. Agarose gels were prepared in PBS at a 0.5% final agarose concentration. NPs at a concentration of 1 μM were incubated with or without 55% plasma in PBS for 15 min, and 2 μL of 50% glycerol was added to the solution to ensure proper gel loading. The mixture was loaded in each well, and the gels were run at a constant voltage of 100 V for 30 min.

Protein Isolation from NPs and SDS-Polyacrylamide Gel Electrophoresis. NP+ and NPs ZMe−ZDiPen (0.5 μM) were incubated in undiluted human serum for 24 h at 37 °C. After incubation, serum−NP mixtures were loaded onto a sucrose cushion (24%) to rapidly separate NP−protein complexes from serum by centrifugation at 14 000 rpm for 30 min.[14] The supernatant was carefully removed, and the residues were washed with 1 mL of PBS three times. Proteins were eluted from the nanoparticles by adding 4× Laemmli sample buffer (Biorad 161-0747) with 2-mercaptoethanol to the pellet and subsequent incubation at 95 °C for 5 min. For 1D gel electrophoresis, 20 μL of recovered proteins in sample buffer was separated on a 12% SDS-PAGE gel. Gels were run at the constant voltage of 150 V for 1 h, and silver staining was performed to visualize the bands according to the previously published protocol.[57] A 0.1% human serum sample was also run for comparison.

Cellular Uptake. MCF7 cells (breast adenocarcinoma) were cultured at 37 °C under a humidified atmosphere of 5% CO_2. The cells were grown in low glucose Dulbecco's modified Eagle's medium (DMEM, 1.0 g/L glucose) containing 10% fetal bovine serum and 1% antibiotics (100 U/mL penicillin and 100 μg/mL streptomycin). For the uptake experiment, 20 000 cells/well were plated in a 48-well plate prior to the experiment. On the following day, cells were washed one time with PBS followed by NP treatment (25 nM/well) and further incubated with or without 10% serum for 3 h (or 24 h). Following incubation, cells were lysed and the intracellular gold amount was measured using inductively coupled plasma mass spectrometry (Elan 6100, PerkinElmer, Shelton, CT, USA). Each cell uptake experiment was done in triplicate, and each replicate was measured five times by ICP-MS. ICP-MS operating conditions are as below: rf power 1600 W; plasma Ar Flow rate, 15 mL/min, nebulizer Ar flow rate, 0.98 mL/min and dwell time, 45 ms.

Hemolysis. Red blood cells were purified from citrate-stabilized human whole blood (pooled, mixed gender) by multiple cycles of centrifugation and dilution in PBS (5000 rpm, 5 min). The purified RBCs were then diluted in 10 mL of PBS and kept on ice during the sample preparation. Then, 0.1 mL of RBC solution was added to 0.4 mL of NP solution in PBS in a 1.5 mL centrifuge tube (Fisher) and mixed gently by pipetting (NPs at a final concentration of 250 and 500 nM). RBCs incubated with PBS and water were used as negative and positive control, respectively. All NP samples as well as controls were prepared in triplicate. The mixture was incubated at 37 °C for 30 min, 6 h, and 24 h while shaking at 150 rpm. After incubation, the solution was centrifuged at 4000 rpm for 5 min and 100 μL of supernatant was transferred to a 96-well plate. The absorbance value of the supernatant was measured at 570 nm using a microplate reader (SpectraMax M2, Molecular Devices) with absorbance at 655 nm as a reference. To determine hemolysis in the presence of plasma, NPs were preincubated in 55% of plasma solution in PBS (v/v) for 30 min at 37 °C. After the preincubation period, 0.1 mL of washed RBCs was added to the solution and further incubated for 24 h. The percent hemolysis was calculated with the absorbance of each sample and the controls using the following formula:

$$\%\text{hemolysis} = (\text{sample} - \text{negative})/(\text{positive} - \text{negative}) \times 100$$

where "negative" and "positive" indicate the absorbance of the negative and the positive controls, respectively. To corroborate that the lack of hemolytic properties was not due to precipitation of NPs in the presence of RBCs, sedimentation experiments were done in PBS both in the presence and in the absence of RBCs. A control with no NPs was used to remove the background. As observed in Figure S23, the differences in the absorbance in the presence and absence of RBCs are not significant, indicating that NPs remained in the solution for both cases.

Cell Viability. The cell viability was determined by alamar blue assay according to manufacturer protocol (Life Technologies, DAL1100). MCF7 cells (15 000 cells/well) were seeded in a 96-well plate 24 h prior to the experiment. On the following day, the old medium was aspirated and the cells were washed with PBS one time. NPs ZMe−ZDiPen (25 nM each) were then incubated with the cells in 10% serum containing media for 24 h at 37 °C. After the incubation period, the cells were washed three times with PBS and 220 μL of 10% alamar blue solution in serum-containing media was added to each well and cells were further incubated at 37 °C for 3 h. After 3 h, 200 μL of solution from each well were taken out and loaded in a 96-well black microplate. Red fluorescence, resulting from the reduction of the alamar blue solution by viable cells, was measured (ex: 560 nm, em: 590 nm) on a SpectroMax M2 microplate reader (Molecular Device). Viability (%) of NP-treated cells was calculated taking untreated cells as 100% viable. All experiments were performed using at least four parallel replicates.

Conflict of Interest: The authors declare no competing financial interest.

Acknowledgment. This work was supported by the grants from the NIH (EB014277) and the Center for Hierarchical Manufacturing (CMMI-1025020).

Supporting Information Available: Nanoparticle synthesis and characterization, and additional experimental details and figures. This material is available free of charge *via* the Internet at http://pubs.acs.org.

REFERENCES AND NOTES

1. Sapsford, K. E.; Algar, W. R.; Berti, L.; Gemmill, K. B.; Casey, B. J.; Oh, E.; Stewart, M. H.; Medintz, I. L. Functionalizing Nanoparticles with Biological Molecules: Developing Chemistries That Facilitate Nanotechnology. *Chem. Rev.* **2013**, *113*, 1904–2074.
2. Mout, R.; Moyano, D. F.; Rana, S.; Rotello, V. M. Surface Functionalization of Nanoparticles for Nanomedicine. *Chem. Soc. Rev.* **2012**, *41*, 2539–2544.
3. Khlebtsov, N.; Dykman, L. Biodistribution and Toxicity of Engineered Gold Nanoparticles: A Review of *In Vitro* and *In Vivo* Studies. *Chem. Soc. Rev.* **2011**, *40*, 1647–1671.
4. Kim, S. T.; Saha, K.; Kim, C.; Rotello, V. M. The Role of Surface Functionality in Determining Nanoparticle Cytotoxicity. *Acc. Chem. Res.* **2013**, *46*, 681–691.
5. He, X. X.; Nie, H. L.; Wang, K. M.; Tan, W. H.; Wu, X.; Zhang, P. F. *In Vivo* Study of Biodistribution and Urinary Excretion of Surface-Modified Silica Nanoparticles. *Anal. Chem.* **2008**, *80*, 9597–9603.
6. Alexis, F.; Pridgen, E.; Molnar, L. K.; Farokhzad, O. C. Factors Affecting the Clearance and Biodistribution of Polymeric Nanoparticles. *Mol. Pharmaceutics* **2008**, *5*, 505–515.
7. Walkey, C. D.; Chan, W. C. W. Understanding and Controlling the Interaction of Nanomaterials with Proteins in a Physiological Environment. *Chem. Soc. Rev.* **2012**, *41*, 2780–2799.
8. Monopoli, M. P.; Aberg, C.; Salvati, A.; Dawson, K. A. Biomolecular Coronas Provide the Biological Identity of Nanosized Materials. *Nat. Nanotechnol.* **2012**, *7*, 779–786.
9. Del Pino, P.; Pelaz, B.; Zhang, Q.; Maffre, P.; Nienhausbc, G. U.; Parak, W. J. Protein Corona Formation Around

Nanoparticles—From the Past to the Future. *Mater. Horiz.* **2014**, *1*, 301–313.
10. Pelaz, B.; Charron, G.; Pfeiffer, C.; Zhao, Y.; de la Fuente, J. M.; Liang, X.-J.; Parak, W. J.; Del Pino, P. Interfacing Engineered Nanoparticles with Biological Systems: Anticipating Adverse Nano–Bio Interactions. *Small* **2013**, *9*, 1573–1584.
11. Mahmoudi, M.; Lynch, I.; Ejtehadi, M. R.; Monopoli, M. P.; Bombelli, F. B.; Laurent, S. Protein Nanoparticle Interactions: Opportunities and Challenges. *Chem. Rev.* **2011**, *111*, 5610–5637.
12. Lundqvist, M.; Stigler, J.; Elia, G.; Lynch, I.; Cedervall, T.; Dawson, K. A. Nanoparticle Size and Surface Properties Determine the Protein Corona with Possible Implications for Biological Impacts. *Proc. Natl. Acad. Sci. U.S.A.* **2008**, *105*, 14265–14270.
13. Aggarwal, P.; Hall, J. B.; McLeland, C. B.; Dobrovolskaia, M. A.; McNeil, S. E. Nanoparticle Interaction with Plasma Proteins as It Relates to Particle Biodistribution, Biocompatibility and Therapeutic Efficacy. *Adv. Drug Delivery Rev.* **2009**, *61*, 428–437.
14. Tenzer, S.; Docter, D.; Kuharev, J.; Musyanovych, A.; Fetz, V.; Hecht, R.; Schlenk, F.; Fischer, D.; Kiouptsi, K.; Reinhardt, C.; *et al.* Rapid Formation of Plasma Protein Corona Critically Affects Nanoparticle Pathophysiology. *Nat. Nanotechnol.* **2013**, *8*, 772–781.
15. Mirshafiee, V.; Mahmoudi, M.; Lou, K. Y.; Cheng, J. J.; Kraft, M. L. Protein Corona Significantly Reduces Active Targeting Yield. *Chem. Commun.* **2013**, *49*, 2557–2559.
16. Salvati, A.; Pitek, A. S.; Monopoli, M. P.; Prapainop, K.; Bombelli, F. B.; Hristov, D. R.; Kelly, P. M.; Aberg, C.; Mahon, E.; Dawson, K. A. Transferrin-Functionalized Nanoparticles Lose Their Targeting Capabilities When a Biomolecule Corona Adsorbs on the Surface. *Nat. Nanotechnol.* **2013**, *8*, 137–143.
17. Lesniak, A.; Fenaroli, F.; Monopoli, M. R.; Aberg, C.; Dawson, K. A.; Salvati, A. Effects of the Presence or Absence of a Protein Corona on Silica Nanoparticle Uptake and Impact on Cells. *ACS Nano* **2012**, *6*, 5845–5857.
18. Zhu, Z. J.; Posati, T.; Moyano, D. F.; Tang, R.; Yan, B.; Vachet, R. W.; Rotello, V. M. The Interplay of Monolayer Structure and Serum Protein Interactions on the Cellular Uptake of Gold Nanoparticles. *Small* **2012**, *8*, 2659–2663.
19. Jokerst, J. V.; Lobovkina, T.; Zare, R. N.; Gambhir, S. S. Nanoparticle PEGylation for Imaging and Therapy. *Nanomedicine* **2011**, *6*, 715–728.
20. Karakoti, A. S.; Das, S.; Thevuthasan, S.; Seal, S. PEGylated Inorganic Nanoparticles. *Angew. Chem., Int. Ed.* **2011**, *50*, 1980–1994.
21. Hamad, I.; Al-Hanbali, O.; Hunter, A. C.; Rutt, K. J.; Andresen, T. L.; Moghimi, S. M. Distinct Polymer Architecture Mediates Switching of Complement Activation Pathways at the Nanosphere–Serum Interface: Implications for Stealth Nanoparticle Engineering. *ACS Nano* **2010**, *4*, 6629–6638.
22. Sekiguchi, S.; Niikura, K.; Matsuo, Y.; Ijiro, K. Hydrophilic Gold Nanoparticles Adaptable for Hydrophobic Solvents. *Langmuir* **2012**, *28*, 5503–5507.
23. Rosen, J. E.; Gu, F. X. Surface Functionalization of Silica Nanoparticles with Cysteine: A Low-Fouling Zwitterionic Surface. *Langmuir* **2011**, *27*, 10507–10513.
24. Yang, W.; Zhang, L.; Wang, S.; White, A. D.; Jiang, S. Y. Functionalizable and Ultra Stable Nanoparticles Coated with Zwitterionic Poly(carboxybetaine) in Undiluted Blood Serum. *Biomaterials* **2009**, *30*, 5617–5621.
25. Cao, Z. Q.; Jiang, S. Y. Super-Hydrophilic Zwitterionic Poly(carboxybetaine) and Amphiphilic Non-ionic Poly(ethylene glycol) for Stealth Nanoparticles. *Nano Today* **2012**, *7*, 404–413.
26. Murthy, A. K.; Stover, R. J.; Hardin, W. G.; Schramm, R.; Nie, G. D.; Gourisankar, S.; Truskett, T. M.; Sokolov, K. V.; Johnston, K. P. Charged Gold Nanoparticles with Essentially Zero Serum Protein Adsorption in Undiluted Fetal Bovine Serum. *J. Am. Chem. Soc.* **2013**, *135*, 7799–7802.
27. McCormick, C. L.; Lowe, A. B. Aqueous RAFT Polymerization: Recent Developments in Synthesis of Functional Water-Soluble (Co)polymers with Controlled Structures. *Acc. Chem. Res.* **2004**, *37*, 312–325.
28. Matyjaszewski, K. Atom Transfer Radical Polymerization (ATRP): Current Status and Future Perspectives. *Macromolecules* **2012**, *45*, 4015–4039.
29. Arvizo, R. R.; Miranda, O. R.; Moyano, D. F.; Walden, C. A.; Giri, K.; Bhattacharya, R.; Robertson, J. D.; Rotello, V. M.; Reid, J. M.; Mukherjee, P. Modulating Pharmacokinetics, Tumor Uptake and Biodistribution by Engineered Nanoparticles. *PLoS One* **2011**, *6*, e24374.
30. Maiti, S.; Das, K.; Dutta, S.; Das, P. K. Striking Improvement in Peroxidase Activity of Cytochrome *c* by Modulating Hydrophobicity of Surface-Functionalized Gold Nanoparticles within Cationic Reverse Micelles. *Chem.—Eur. J.* **2012**, *18*, 15021–15030.
31. Zuo, G.; Huang, Q.; Wei, G.; Zhou, R.; Fang, H. Plugging into Proteins: Poisoning Protein Function by a Hydrophobic Nanoparticle. *ACS Nano* **2010**, *4*, 7508–7514.
32. Fubini, B.; Ghiazza, M.; Fenoglio, I. Physico-Chemical Features of Engineered Nanoparticles Relevant to Their Toxicity. *Nanotoxicology* **2010**, *4*, 347–363.
33. Chompoosor, A.; Saha, K.; Ghosh, P. S.; Macarthy, D. J.; Miranda, O. R.; Zhu, Z. J.; Arcaro, K. F.; Rotello, V. M. The Role of Surface Functionality on Acute Cytotoxicity, ROS Generation and DNA Damage by Cationic Gold Nanoparticles. *Small* **2010**, *6*, 2246–2249.
34. Moyano, D. F.; Goldsmith, M.; Solfiell, D. J.; Landesman-Milo, D.; Miranda, O. R.; Peer, D.; Rotello, V. M. Nanoparticle Hydrophobicity Dictates Immune Response. *J. Am. Chem. Soc.* **2012**, *134*, 3965–3967.
35. Kreuter, J.; Liehl, E.; Berg, U.; Soliva, M.; Speiser, P. P. Influence of Hydrophobicity on the Adjuvant Effect of Particulate Polymeric Adjuvants. *Vaccine* **1988**, *6*, 253–256.
36. Zhang, G.; Yang, Z.; Lu, W.; Zhang, R.; Huang, Q.; Tian, M.; Li, L.; Liang, D.; Li, C. Influence of Anchoring Ligands and Particle Size on the Colloidal Stability and *In Vivo* Biodistribution of Polyethylene Glycol-Coated Gold Nanoparticles in Tumor-Xenografted Mice. *Biomaterials* **2009**, *30*, 1928–1936.
37. Rana, S.; Yu, X.; Patra, D.; Moyano, D. F.; Miranda, O. R.; Hussain, I.; Rotello, V. M. Control of Surface Tension at Liquid–Liquid Interfaces Using Nanoparticles and Nanoparticle–Protein Complexes. *Langmuir* **2012**, *28*, 2023–2027.
38. Xiao, Y.; Wiesner, M. R. Characterization of Surface Hydrophobicity of Engineered Nanoparticles. *J. Hazard. Mater.* **2012**, *215*, 146–151.
39. Zhang, C.; Macfarlane, R. J.; Young, K. L.; Choi, C. H. J.; Hao, L.; Auyeung, E.; Liu, G.; Zhou, X.; Mirkin, C. A. A General Approach to DNA-Programmable Atom Equivalents. *Nat. Mater.* **2013**, *12*, 741–746.
40. Milani, S.; Bombelli, F. B.; Pitek, A. S.; Dawson, K. A.; Rädler, J. Reversible *versus* Irreversible Binding of Transferrin to Polystyrene Nanoparticles: Soft and Hard Corona. *ACS Nano* **2012**, *6*, 2532–2541.
41. Casals, E.; Puntes, V. F. Inorganic Nanoparticle Biomolecular Corona: Formation, Evolution and Biological Impact. *Nanomedicine* **2012**, *7*, 1917–1930.
42. Monopoli, M. P.; Pitek, A. S.; Lynch, I.; Dawson, K. A. Formation and Characterization of the Nanoparticle–Protein Corona. *Methods Mol. Biol.* **2013**, *1025*, 137–155.
43. Zhu, Z.-J.; Ghosh, P.; Miranda, O. R.; Vachet, R. W.; Rotello, V. M. Multiplexed Screening of Cellular Uptake of Gold Nanoparticles Using Laser Desorption/Ionization Mass Spectrometry. *J. Am. Chem. Soc.* **2008**, *130*, 14139–14143.
44. Mortimer, G. M.; Butcher, N. J.; Musumeci, A. W.; Deng, Z. J.; Martin, D. J.; Minchin, R. F. Cryptic Epitopes of Albumin Determine Mononuclear Phagocyte System Clearance of Nanomaterials. *ACS Nano* **2014**, *8*, 3357–3366.
45. Walkey, C. D.; Olsen, J. B.; Song, F.; Liu, R.; Guo, H.; Olsen, D. W. H.; Cohen, Y.; Emili, A.; Chan, W. C. W. Protein Corona Fingerprinting Predicts the Cellular Interaction of Gold and Silver Nanoparticles. *ACS Nano* **2014**, *8*, 2439–2455.

46. Walkey, C. D.; Olsen, J. B.; Guo, H.; Emili, A.; Chan, W. C. Nanoparticle Size and Surface Chemistry Determine Serum Protein Adsorption and Macrophage Uptake. *J. Am. Chem. Soc.* **2012**, *134*, 2139–2147.
47. Gessner, A.; Waicz, R.; Lieske, A.; Paulke, B. R.; Mader, K.; Muller, R. H. Nanoparticles with Decreasing Surface Hydrophobicities: Influence on Plasma Protein Adsorption. *Int. J. Pharm.* **2000**, *196*, 245–249.
48. Baier, G.; Costa, C.; Zeller, A.; Baumann, D.; Sayer, C.; Araujo, P. H. H.; Mailander, V.; Musyanovych, A.; Landfester, K. BSA Adsorption on Differently Charged Polystyrene Nanoparticles Using Isothermal Titration Calorimetry and the Influence on Cellular Uptake. *Macromol. Biosci.* **2011**, *11*, 628–638.
49. Patil, S.; Sandberg, A.; Heckert, E.; Self, W.; Seal, S. Protein Adsorption and Cellular Uptake of Cerium Oxide Nanoparticles as a Function of Zeta Potential. *Biomaterials* **2007**, *28*, 4600–4607.
50. Kim, C. K.; Ghosh, P.; Pagliuca, C.; Zhu, Z.-J.; Menichetti, S.; Rotello, V. M. Entrapment of Hydrophobic Drugs in Nanoparticle Monolayers with Efficient Release into Cancer Cells. *J. Am. Chem. Soc.* **2009**, *131*, 1360–1361.
51. Hühn, D.; Kantner, K.; Geidel, C.; Brandholt, S.; Cock, I. D.; Soenen, S. J. H.; Rivera_Gil, P.; Montenegro, J.-M.; Braeckmans, K.; Müllen, K.; *et al.* Polymer-Coated Nanoparticles Interacting with Proteins and Cells: Focusing on the Sign of the Net Charge. *ACS Nano* **2013**, *7*, 3253–3262.
52. Fleischer, C. C.; Kumar, U.; Payne, C. K. Cellular Binding of Anionic Nanoparticles is Inhibited by Serum Proteins Independent of Nanoparticle Composition. *Biomater. Sci.* **2013**, *1*, 975–982.
53. Xiao, W. C.; Lin, J.; Li, M. L.; Ma, Y. J.; Chen, Y. X.; Zhang, C. F.; Li, D.; Gu, H. C. Prolonged *In Vivo* Circulation Time by Zwitterionic Modification of Magnetite Nanoparticles for Blood Pool Contrast Agents. *Contrast Media Mol. Imaging* **2012**, *7*, 320–327.
54. Lin, Y. S.; Haynes, C. L. Impacts of Mesoporous Silica Nanoparticle Size, Pore Ordering, and Pore Integrity on Hemolytic Activity. *J. Am. Chem. Soc.* **2010**, *132*, 4834–4842.
55. Lin, Y. S.; Haynes, C. L. Synthesis and Characterization of Biocompatible and Size-Tunable Multifunctional Porous Silica Nanoparticles. *Chem. Mater.* **2009**, *21*, 3979–3986.
56. Saha, K.; Moyano, D. F.; Rotello, V. M. Protein Coronas Suppress the Hemolytic Activity of Hydrophilic and Hydrophobic Nanoparticles. *Mater. Horiz.* **2014**, *1*, 102–105.
57. Chevallet, M.; Luche, S.; Rabilloud, T. Silver Staining of Proteins in Polyacrylamide Gels. *Nat. Protoc.* **2006**, *1*, 1852–1858.